The real-time interaction model for transient mode investigations of a dual-piston free-piston engine generator

M. Razali Hanipah [a,b]*, R. Mikalsen , A.P. Roskilly [c]

[a]Centre for Automotive Engineering, Universiti Malaysia Pahang,
26600, Pekan, Pahang, Malaysia
[b]Department of Mechanical Engineering, College of Engineering, Universiti Malaysia Pahang,
26300 Gambang, Pahang, Malaysia.
[c]Department of Engineering, Durham University, Durham DH1 3LE, United Kingdom

* Corresponding author. Email: mohdrazali@ump.edu.my

Abstract

A free-piston engine generator is being developed worldwide as a novel means of electrical power generator for light vehicle application, which can provide a complementary solution towards reducing carbon dioxide emissions of road vehicles in general. However, the absence of a crank-slider mechanism in free-piston engines resulted in poor transient operations. Transient real-time modelling and simulation can provide the interaction between in-cylinder combustion with dynamics of piston motion, which has not been fully explored previously. This paper presents a real-time interaction model between dynamics of the piston motion and thermodynamics of the in-cylinder combustion of a two-stroke spark ignition dual-piston free-piston engine generator for transient operation investigations. The simulation model was developed based on the working prototype and comprised of zero- and one-dimensional sub-models interacted in real-time governed by a single timestep. The study focuses on three critical transient modes: motoring, starting and generating for the transient performance investigation. A series of experimental results during motoring was used for validating the simulation model, which showed good agreement between simulation and experiment results with 2-5% errors. The targeted brake thermal efficiency is around 20~30% at 50~60 Hz engine speed which has been shown achievable. Transient speeds of 10 and 25 Hz produced higher combustion pressure around the top dead centre but suffered pumping loss at the end of the expansion stroke. The lower peak pressures at 50 and 60 Hz have contributed to the lower brake mean effective pressure values. Maximum brake thermal efficiency of 25.8% lies in the mid-range of compression ratios between 10:1 to 15:1 while at the cyclic speeds of 50Hz to 60Hz. Maximum brake mean effective pressure contour occurs between 5 to 12.5 compression ratios and corresponding speeds of 10 to 30 Hz. It was observed that the excess energy from combustion results in piston overshoot condition while insufficient energy prevents the piston from achieving the targeted stroke and compression ratio. Knock events were observed for high compression ratio cases regardless of engine speed. Predictive stroke control and knock detection capability are the main contribution of the real-time interaction model presented in this paper for realistic transient operation investigation and performance prediction of the dual-piston free-piston engine generator.

Keywords: free-piston engine generator; transient performance investigation; real-time numerical simulation; predictive stroke control; cyclic position

1 Overview

Coupling an internal combustion engine with an electrical power generator is not new. The crankshaft internal combustion engine has long been the prime mover for portable power generators and hybrid electric vehicles. In the recent decade, the research toward crank-less linear engines known as the free-piston engine has been heavily investigated [1], [2].

Free-piston has a long history which conceptually begins with Otto-Langen atmospheric free-piston engine in 1867 [3], [4]. This early prototype of a free-piston engine was meant for rotary applications, made possible using rack and pinion mechanisms. Pescara patented the following modern free-piston engine concept around 1922 for the application of air compressors and gas generators [5]. Junkers successful opposed-piston free-piston gas compressor, known for its excellent stability [6], was a wide application throughout the German navy circa the 1940s [7]. Innas free-piston engine introduced by Achten [8] has reported a promising potential for the hydraulic free-piston engine against a conventional engine-pump [9].

A free-piston engine generator (FPEG) converts the chemical energy through the combustion process into kinetic energy of the moving mass and finally into electrical energy through the integrated generator. This electrical energy can be stored in an energy storage system for various applications. One of the vital motivations of the recent efforts in FPEG development is arguably the potential of a free-piston engine generator to provide a compact and efficient power generator for hybrid electric vehicles [2].

FPEG inherit variable compression ratio capability with fewer modifications than conventional crankshaft engine, hence is suitable for multi-fuel operation [10]. Further, its high efficiency and rapid transient response ma it ideal for hybrid electric vehicle application [11]. Further advantages include high thermal efficiency and power to weight ratio, low manufacturing cost, low maintenance due to fewer components, and mechanical simplicity [12], [13].

Generally, the free-piston engine design can be categorised into three main configurations as reported by Aichlmayr [14], Achten [8] and Mikalsen and Roskilly [10]. A single-piston type free-piston engine is the primary design comprised of a single-piston, single combustion chamber, a load and a rebound device. This design is mainly employed for air compressor and hydraulic pump applications [8], [10]. Thus, the load and rebound devices in those applications can be integrated. This configuration is the most straightforward FPE design and easier to control, but it is not mechanically balanced [14].

An opposed-piston type free-piston engine comprises two opposing single-piston configurations linked together with a synchronising linkage. A common combustion chamber is in the middle, while each piston can have its load and rebound device. It has been reported in compressor[6], gasifier [15] and hydraulic applications [16]. This design is inherently balanced when symmetrically designed, with equal masses of pistons and synchronising linkage added [10], [14]. However, the overall design is more complex and bulkier than single or dual piston type. Further, the synchroniser linkage poses additional frictional losses and constrains the piston mechanically; hence it is not precisely a 'free-piston' design in literal form.

There are two combustion chambers in a dual-piston type configuration, and a single load is placed in the middle without any rebound device. Each combustion chamber will act as the rebound device alternately during the cyclic operation. It has been reported for electrical generator [17]–[19] and hydraulic application [20]. The main advantages of this design are that it produces power in each stroke, and there is no need for a rebound device. The challenges for this design are in terms of mechanical vibrations and the need for piston motion control. Further, since each combustion chamber serves as a rebound device, the piston motion control becomes more complicated as more control variables are introduced in the system.

The researchers in Sandia National Laboratory [21], [22] have demonstrated the ideal Otto cycle behaviour of the free-piston engine using a numerical study and a series of single-shot experiments. Furthermore, the rapid compression expansion machine (RCEM) experiments had shown that it is possible to achieve an indicated thermal efficiency of 56% with low emissions and a very lean fuel-air mixture at a 30:1 compression ratio [17].

The researchers at the Royal Institute of Technology (KTH) have investigated free-piston energy converter (FPEC). The FPEC was designed for the application of a Hybrid Electric Vehicle (HEV) with a 45kW power output capacity. MATLAB-Simulink modelling simulations results showed that the efficiency was 5-10% better than diesel electrical generator at different load ranges [23].

The researchers from the Chalmers University of Technology had simulated the FPEC piston dynamic using MATLAB-Simulink with two main sub-models. The gas exchange was calculated using BOOST, and the chemical reaction was simulated in SENKIN. The fuel-to-electricity efficiency of the FPEC was found to range from 41.9–44.4% [24]. Further, a numerical study of HCCI free-piston energy converter (FPEC) developed for vehicle propulsion was shown to achieve an indicated efficiency of 51% [25].

A spark ignition (SI) and compression ignition (CI) free-piston generator were numerically investigated by Mikalsen and Roskilly [26], [27]. Both models were created using C++ and implemented in OpenFOAM. The indicated thermal efficiency of the free-piston generator was higher than the conventional engine at lower engine speed (below 3000 rpm), found to be peaked at 32.6% [26]. The CI version was simulated in HCCI mode and had achieved almost 50% indicated thermal efficiency [27].

The inconsistent piston position in the free-piston engine generator, especially during transient operation, has prevented this technology from being successfully developed and tested by various research groups [1], [28]. Motion characterisation has been identified as the stepping stone towards developing a robust algorithm for a stable FPEG operation [29], [30]. This is because the absence of a crank-slider mechanism in the free-piston engine has resulted in erratic piston positioning during starting and loading [28], [31], [32]. Due to the limitation of the simulation tools employed, the simulation models developed by various researchers focused on either the electrical aspect or the mechanical aspects. Co-simulation between internal combustion engine model, dynamics model and controller sub-model will produce an accurate piston motion dynamics and in-cylinder pressure development for the purpose of motion characterisation for predictive control during the transient operation.

As a result, the free-piston engine control system has increasingly become more complicated and require advanced multi-physics models. The researchers from Czech Technical University (CTU) had presented the modelling and control of the free-piston-generator engine [33]. A nonlinear time-based in-cycle thermodynamic model of the linear combustion engine (LCE) was developed and simulated using MATLAB Simulink [34]. A recent co-simulation between Ricardo WAVE and MATLAB Simulink has been proposed [19], [35].

A predictive motion controller was proposed by Mikalsen et al. [30] to improve the dynamic response of the controller. This strategy can be implemented via the real-time controller. In addition, the main objective of this strategy is to avoid extremely high and low pressure in the cylinders by appropriate intervention via fuel mass flow and ignition timing. Thus, the braking of the electrical generator could be minimised to avoid component failures.

In addition, it has been shown through simulations that the free-piston engine is very sensitive to rapid load change, thus severely affecting the controller performance [36]. Thus, with a fundamental assessment of the FPEG system equation of motion, further understanding of the motion control requirements for the controller can be obtained.

From this past research, it can be summarised that; modelling and simulation are key elements in FPEG control system optimisation, and it has been commonly modelled using zero-dimensional models to obtain the piston dynamics and predict engine performance. Many of the numerical models were developed in MATLAB Simulink, and multiple sub-systems were required to represent each equation.

Dual-piston type FPEG is the primary choice amongst various research groups and has been the subject of modelling and simulation investigations throughout the years [2]. Regardless, due to its complex interactions, internally within the cylinder and externally with the integrated generator, numerical simulation remains the most cost-effective approach in looking into the subject. One of the most challenging aspects of the FPEG is the transient operation and performance. This paper presents a real-time interaction free-piston engine model with

3

predictive stroke control for transient operation investigations. This model illustrates the various phases of transient operations for a free-piston engine generator with predictive stroke control. The model can predict the knock phenomenon, which can aid in stroke control for future hardware in the loop (HIL) development stage.

2   Free-Piston Engine Generator Fundamentals

The free-piston engine works on dynamic forces balance while producing linear reciprocation motion. This engine is dynamically constrained instead of a kinematically constrained crank-slider engine [14]. Further, the fundamental principle of operation of FPE requires a new approach due to the absence of the crank-slider mechanism.
Primarily, for a continuous cyclic operation to be possible, the free-piston engine requires a bounce chamber to ensure the piston returns to the initial top-dead-centre position for the subsequent cycle. This bounce chamber can be in the form of a second combustion chamber [37], [38], compressed air storage [39] or hydraulic fluid storage [9].

The absence of a crank-slider mechanism also means conventional flywheel and crankshaft counterbalance are no longer available as energy storage and cyclic fluctuation dampener. It creates a critical issue since the engine must obtain energy from each stroke since there is no flywheel. Thus, researchers have suggested that the integrated linear motor operation assists in misfire [38], [40]. Such an approach requires new means of monitoring the translational displacement and in-cylinder pressure at a very high acquisition speed and processing power to enable the control system to intervene precisely.

In terms of the engine cycle, the free-piston engine must operate in a two-stroke cycle, although the four-stroke cycle version was theoretically possible [41]–[43]. The two-stroke version is widely adopted since combustion occurs at every stroke to provide expansion energy required for reciprocation, increasing its power density.

This section looks at the fundamentals of free-piston engine generator governing equations. These equations were employed in the transient model developed in this research.

2.1   Free-piston dynamics and forces

Newton second law has been applied by various researchers [40], [44]–[46] to model the dynamics of the free-piston engine. It is limited to the single piston and dual-piston configuration since the opposed piston requires a synchroniser mechanism that introduces kinematic constraint to the pistons. Hence, it should be treated like a crankshaft engine. The free-piston engine generator (FPEG) converts the chemical energy of the fuels through the combustion process into kinetic energy of the moving mass and finally into electrical energy through the integrated generator. This electrical energy can then be stored in an energy storage system for various applications.
The dynamic model of the FPEG, which is shown in **Fig. 1**, comprises of:
the in-cylinder pressure forces acting on both cylinders, F_{p_1} and F_{p_2}
the frictional forces due to contact surfaces on the moving part of the engine, F_f
the net force or inertial load of the moving mass, $m\ddot{x}$
the cogging force acting on the permanent magnet assembly of the generator, F_{cog}
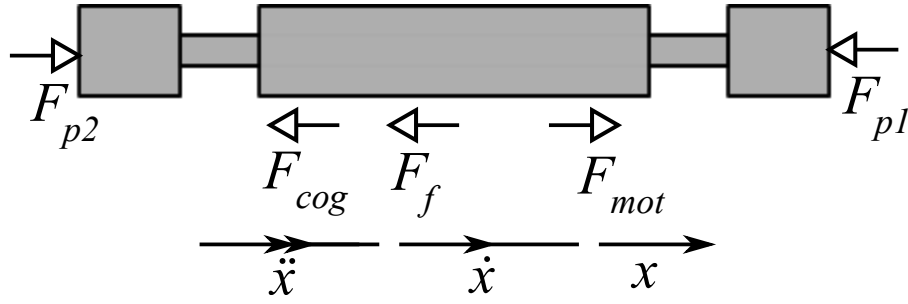the motoring force energised during starting, F_{mot}

Fig. 1. The dual piston free-piston engine generator components layout and free-body diagram of the dynamic model

These forces which analysed using Newton second law of motion and can be summarised as:

$$\sum F = F_{mot} + F_p - F_f - F_{cog} = m\ddot{x} \qquad 1$$

Where $\ddot{x}$ is the acceleration of the piston in the direction of motion and m moving mass. The moving mass includes the mass of piston assembly, translator and magnet assembly. While F_p is the resultant in-cylinder pressure forces acting on the translator can be expressed as:

$$F_p = F_{p_1} - F_{p_2} = (p_1 - p_2) \times \frac{\pi B^2}{4} \qquad 2$$

2.1.1 Motoring force

The free-piston linear generator can be operated as a linear motor by injecting electrical current to produce the reciprocation motion. During this process, the switching between each coil is determined from the linear position reading and must occur at precise timing and position to produce a consistent motoring force during starting.

The motoring force is determined from the linear motor force constant (K_f) which is inherited in the stator coil and depends on the winding type. Based on Lorentz law, the motoring force generated for delta and Y winding can be evaluated as follows [47]:

$$F = I_{phase} \times K_{f-\Delta} \qquad 3$$

$$F = \sqrt{3} \times I_{phase} \times K_{f-Y} \qquad 4$$

The required motoring force is determined from the cyclic speed [48]. A targeted compression ratio can be achieved at a very low speed with the risk of increasing coil temperature as the high current flows longer in the coil during motoring [49]. However, low-speed motoring produces poor scavenging and increases blow-by reducing final compression pressure.

2.1.2 Frictional force

The frictional force in a free-piston engine generator is often simplified in the simulation models since it is less without the crank mechanism. The frictional force is assumed to be constant throughout the cycle by most researchers, but better modelling has been provided by Atkinson [45] from the empirical formula provided by Blair [50], which can be simplified into:

$$F_f = 3150 \cdot V_d \cdot f \qquad 5$$

For modelling purposes, the equation above is sufficient since it relates cylinder size through the displacement volume (V_d) and engine frequency (f). From this equation, the frictional force is minimal (less than 6 N) and thus assumed to be a part of the load as previously done [45].

Goldsborough and Blarigan [51] have modelled the frictional force by including both static and viscous components (f_1 and f_2) as follows:

$$F_f = sign(v_p)[f_1 + f_2|v_p|] \qquad 6$$

This equation can accurately represent any prototype since f_1 and f_2 are determined experimentally and unique to the prototype being tested.

The friction model is a modified form of the Chen-Flynn correlation [52] as shown in Equation 7, where the first term represents accessory (e.g. water pump, alternator and condenser) friction, the second term varies with peak cylinder pressure, the third term represents hydrodynamic friction, and the fourth term represents windage losses.

$$f_{mep} = A_{cf}V_c + \frac{1}{ncyl} \sum_{i=1}^{ncyl} \left[B_{cf}(P_{max})_i + C_{cf} * (S_{fact})_i + Q_{cf}(S_{fact})_i^2 \right] \qquad 7$$

with:

$$S_{fact} = N_{rpm}\left(\frac{S}{2}\right) \qquad 8$$

2.2   Thermodynamics consideration

2.2.1   Cylinder parameters

The terms and definitions used in this section is a combination of information obtained from Heywood [4], Blair [53] and Pulkrabek [54] for crankshaft engines.

The definitions for combustion chamber and cylinder geometry are shown in Fig. **2**. The diameter of the cylinder is the bore (B). The stroke (S) is defined as the distance travelled by the piston from (bottom dead centre) BDC to (top dead centre) TDC, and the volume within the stroke is known as the swept volume (V_s). For a free-piston engine, the nominal stroke (S_{nom}) will be defined instead as the stroke length is not constant. When the piston is at TDC, the remaining space between the top of the piston and the cylinder head is known as the clearance volume (V_c), which is contained within the clearance distance (c).
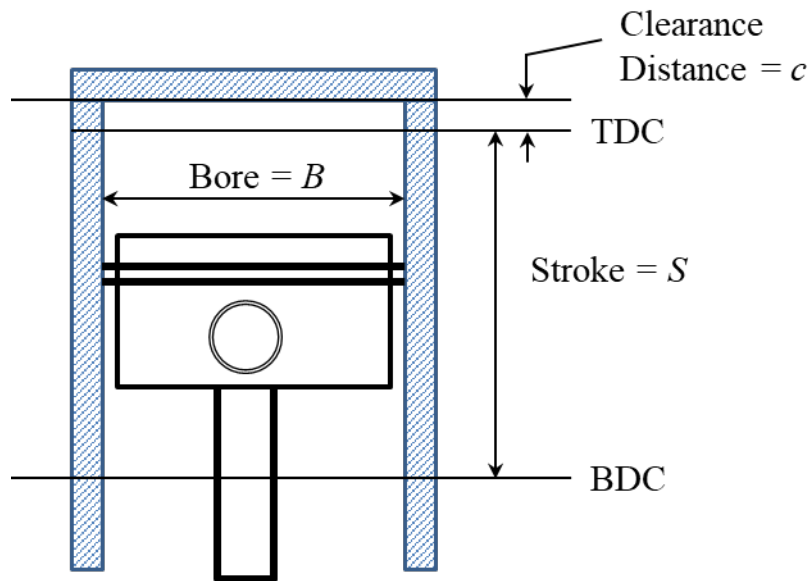

Fig. 2. Cylinder geometry definitions for an engine with a flat top piston (without the bowl).

Further parameters and definitions are given by the following equations:
Swept volume, V_s:

$$V_s = \frac{(\pi B^2 S)}{4} \qquad 9$$

For a known clearance volume (V_c) above the piston at TDC:
Geometric Compression Ratio, $(CR)_G$ is defined as:

$$(CR)_G = \frac{(V_s + V_c)}{V_c} \qquad\qquad 10$$

Next, the clearance volume of each cylinder can be estimated from the geometric compression ratio $(CR)_G$ value input:

$$V_c = \frac{V_s}{((CR)_G - 1)} \qquad\qquad 11$$

Then, the instantaneous volume in the cylinder at each time step can be calculated:

$$V = V_c + \frac{\pi}{4}B^2 s \qquad\qquad 12$$

2.2.2   Air-fuel ratio, fuel-air ratio, lambda and equivalence ratio

In a two-stroke spark-ignition engine, the in-cylinder mixture trapped prior to combustion will determine the in-cylinder pressure development during the power stroke up until the exhaust blowdown. For a carburetted or port fuel injection system, this mixture is assumed to be homogenous. Thus, it is essential to understand the property of this air-fuel mixture (i.e. the reactants) and its impact on combustion.

The composition of these reactants is defined according to Heywood [4], and all the essential parameters related to spark ignition gasoline engines are defined in this section.

The air-fuel ratio (AFR) and fuel-air ratio (FAR) can be defined as follow:

$$AFR = \frac{m_a}{m_f} \qquad\qquad 13$$

The actual mixture will vary from lean (excess air) to rich (excess fuel) compositions. This brings about the following normalised parameters as follow:

The fuel-air equivalence ratio:

$$\phi = \frac{(FAR)_{actual}}{(FAR)_{stoich}} \qquad\qquad 14$$

i.e. FAR is the reciprocal of AFR.

The relative air-fuel ratio, widely known as Lambda:

$$\lambda = \phi^{-1} = \frac{(AFR)_{actual}}{(AFR)_{stoich}} \qquad\qquad 15$$

At the stoichiometric condition, $\lambda = \phi = 1$, for rich mixture, $\phi > 1$ and $\lambda < 1$. For lean mixture, $\phi < 1$ and $\lambda > 1$.

Lean operation is preferred to reduce fuel consumption and HC emissions as long as NO_x emission is under control. However, there are certain operating conditions that require rich mixtures, such as starting, especially during cold cranking and during drastic load change.

2.2.3   Woschni heat transfer

Woschni heat transfer relationship was used to calculate the amount of heat transfer to and from the cylinder charge. In this correlation, the charge is assumed to have a uniform heat flow coefficient and velocity on all surfaces of the cylinder.

$$h_g = 0.0128 B^{-0.20} P^{0.80} T^{-0.53} v_c{}^{0.8} C_{enht} \qquad\qquad 16$$

The characteristic velocity is the sum of the mean piston speed and an additional combustion-related velocity that depends on the difference between the combustion and motoring pressure.

2.2.4   Compression-expansion process

In this calculation, the compression process was governed by a thermodynamic equation for a polytropic process with a constant index. The pressure and temperature at the beginning of the compression have the same values as the corresponding parameters at the end of the scavenging process or ambient conditions. In the two-stroke engine model, the intake valve

closes last during compression, whereas its exhaust valve opens first during expansion. The pressure, p, during the compression process, is given as a function of piston position, x.

The pressure in cylinder 1 at any time t during compression, $p_1(t)$, is:

$$p_1(t) = p_a * \left(\frac{x_{ivc1}}{x_1(t)}\right)^{\gamma_c} \qquad 17$$

Similarly, the pressure in cylinder 2 at any time t during compression, $p_2(t)$, is:

$$p_2(t) = p_a * \left(\frac{L - x_{ivc2}}{x_2(t) - x_{ivc2}}\right)^{\gamma_c} \qquad 18$$

Where:

p_a is the intake air pressure
$x_1(t)$ is the piston position in cylinder 1 at time t
$x_2(t)$ is the piston position in cylinder 2 at time t
x_{ivc1} is the piston position of cylinder 1 when the intake valve is fully closed
x_{ivc2} is the piston position of cylinder 2 when the intake valve is fully closed
L is the ultimate stroke
γ_c is the compression polytropic index

2.2.5 SI Wiebe Combustion

The SI Wiebe function was used to describe the rate of fuel mass burned, which has been observed in any premixed SI combustion obtained experimentally.

In order to solve the dynamics and the polytropic equations, Atkinson et al. [45] have applied the following thermodynamics relationship for the instantaneous in-cylinder pressure; p, instantaneous cylinder volume; V, heat input; Q_{in}, specific heat ratios; γ, and mass fraction burned rate; $\dot{\chi}$, as shown :

$$\dot{p} = -\gamma \cdot \frac{p}{V} \cdot \dot{V} + (\gamma - 1)\frac{Q_{in}}{V}\dot{\chi} \qquad 19$$

A function for the mass fraction burned must be assumed To solve this equation, namely, the Wiebe function. For a free-piston engine, the Wiebe function is expressed as a function of time. The burned rate at a particular instant of time (t) is shown. Where the start of combustion; t_s, combustion duration; C_d, a and b as the adjustable shape parameters obtained from Heywood [4].

$$\chi = 1 - exp\left[-a \cdot \left(\frac{t - t_s}{C_d}\right)^{b+1}\right] \qquad 20$$

2.2.6 Knock calculation

Knock is the auto-ignition of the air-fuel mixture, which raises the cylinder pressure ahead of the downstroke motion of the piston. This entails the loss of combustion energy or damage to the piston. In this model, knock prediction is essential to illustrate the susceptibility of the SI free-piston engine during transient operation. The knock sub-model is based on the Douaud and Eyzat [55] auto-ignition delay correlation for SI engines.

This is done by calculating the auto-ignition delay time in seconds at every timestep using the following equation:

$$\tau = \frac{0.01869}{E_p} * \left(\frac{N_{Oct}}{100}\right)^{3.4107} * p^{-1.7} \exp\left(\frac{\frac{3800}{A_T}}{T}\right) \qquad 21$$

where:

E_p = pre-exponential multiplier
N_{Oct} = User-entered fuel octane number
p = Cylinder pressure [kgf/cm2]
A_T = activation temperature multiplier
T = Unburned gas temperature [K]

8

Generally, auto-ignition delay decreases as combustion progresses and the temperature in the unburned zone rises. Knock incident occurs if the ignition delay is less than the flame arrival time.

Mathematically, the model assumes that auto-ignition occurs when:

$$\int_{t0}^{ti} \frac{d\tau}{\tau} = 1 \qquad\qquad 22$$

where: $t0 =$ start of end-gas compression
        $ti =$ Time of auto-ignition
        $\tau =$ Auto-ignition delay time, defined previously

The fuel burn rate in the post-knock period is assumed to be constant and is calculated as:

$$\dot{m}_{fuel} = \frac{m_{fvapor} + m_{fliquid}}{\tau_{postknock}} \qquad\qquad 23$$

Air is burned proportionally at a rate given by:

$$\dot{m}_{air} = \dot{m}_{fuel} * \left(\frac{A}{F}\right) \qquad\qquad 24$$

where:
$m_{fvapor} =$ Unburned fuel vapour mass at the time of knock
$m_{fliquid} =$ Unburned fuel liquid mass at the time of knock

The result is reported as knock intensity which is defined as:

$$Knock\ Intensity = \frac{Unburned\ mass}{Total\ cylinder\ mass} \qquad\qquad 25$$

2.3   Performance parameters

The processes that occur inside the cylinder of a free-piston engine generator are similar to those of a crankshaft engine. Thus, performance parameters such as mean effective pressure and thermal efficiency have been reported for free-piston engines [21], [45].

This section will first review the theoretical definitions of these performance parameters and then present engine performance investigations conducted using the 1-D simulation model.

2.3.1   Work, power, mean effective pressure and efficiency

The work done per cycle for a two-stroke engine can be calculated from the integration of the area under the pV curve.

Mean effective pressure is defined as the work per cycle of an engine divided by the cylinder volume displaced per cycle [4]. It is a useful performance parameter for comparing different types of engines since it is independent of engine size and is given by the following equation:

$$mep = \frac{\text{work per cycle}}{\text{displacement volume}} \qquad\qquad 26$$

There are two main types of mep, namely indicated mean effective pressure ($imep$) and brake mean effective pressure ($bmep$). Virtually, $imep$ can be represented by a constant pressure applied on the piston from BDC to TDC, which will produce the same amount of work per cycle [53].

Indicated power can be determined from the same pressure versus volume graph at a specific engine speed according to the following equation:

$$P_i = \oint pdV \times N \qquad\qquad 27$$

Where N is the engine speed in revolution per second.

Alternatively, the indicated power can be determined from $imep$ as follow:

$$P_i = imep \times V_s \times N \qquad\qquad 28$$

Although the brake quantities can only be obtained via engine testing, the following relationships can also be used in relation to the indicated quantities [53], [54] :

$$P_b = P_i - P_{tf} \qquad\qquad 29$$
$$bmep = imep - tfmep \qquad\qquad 30$$

$$bmep = \sum_{cylinder} \frac{\oint pdV}{V_s} + \sum_{crankcase} \frac{\oint pdV}{V_s} - tfmep \qquad\qquad 31$$

Where:

$tfmep$ = Total friction mean effective pressure

The total friction mean effective pressure ($tfmep$) is defined as follow:

$$tfmep = pmep + rfmep + amep \qquad\qquad 32$$

Torque is an essential performance parameter for a crankshaft engine which can be obtained from engine dynamometer testing that reflects the engine's ability to do work [4], [53], [54]. However, the free-piston engines produced no torque since there was no crankshaft. Therefore, in this research, $bmep$ and brake power are used for assessing its ability to do work as given from the following relationship with the torque:

$$bmep = \frac{\tau \times 2\pi}{V_s} \qquad\qquad 33$$

Engine efficiency is another performance parameter used in assessing both models in the performance investigation. Thermal efficiency is the ratio of work output per energy input as given in the following equation for indicated thermal efficiency:

$$\eta_i = \frac{P_i}{\dot{Q}_{in}} = \frac{P_i}{(Q_{HV}) \times (\eta_c) \times (\dot{m}_f)} \qquad\qquad 34$$

Combustion efficiency is the measure of the fraction of fuel burnt during the combustion process, and typical values are 0.95 to 0.98 [4]. The theoretical relationship for the combustion efficiency in terms of enthalpy of the reactants (air and fuel) and the products (exhaust gases) is given as (as presented by Heywood [4], see also Matthews [56]):

$$\eta_c = \frac{H_R(T_A) - H_P(T_A)}{m_f \times Q_{HV}} \qquad\qquad 35$$

In the actual engine operation, the reactants can be in the form of a lean mixture (excess air) which will produce a smaller amount of incomplete combustion products or a rich mixture (excess fuel) which increases these amounts [4]. For this reason, combustion efficiency must be determined from experiments by measuring the fuel flow and airflow into the engine as well as exhaust gas flow, exhaust gas compositions and oxygen content, as explained by Blair [53].

Similarly, brake thermal efficiency, η_b, is defined as follow:

$$\eta_b = \frac{P_b}{\dot{Q}_{in}} = \frac{P_b}{(Q_{HV})(\eta_c)(\dot{m}_f)} \qquad\qquad 36$$

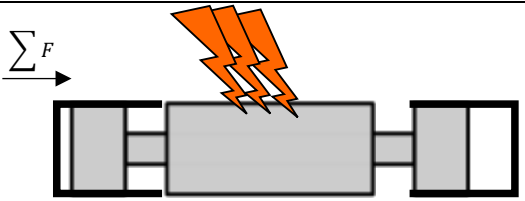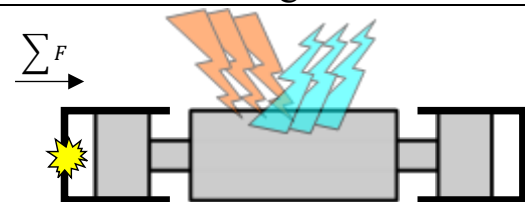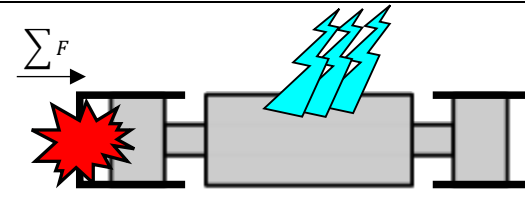Where: P_b is the brake power output produced by the engine [W]

3   Real-time interaction transient model approach

A real-time interaction model has been developed for looking into the transient behaviour of free-piston engine dynamics. The model involves interaction between dynamics of the piston motion and thermodynamics of the in-cylinder combustion. In this way, the negative impact of piston dynamics on combustion can be mitigated for sustainable operation.

3.1   Transient modes

Generally, free-piston engine generator transient operations can be distinguished in three modes, as summarised in Table 1. These transient operations are the main phases that an FPEG must go through during the operation. First is the motoring mode, which occurred during starting, with the motoring force being the most dominant force. During motoring mode, the aim is to obtain cyclic speed for gas exchange and sufficient cylinder pressure for combustion. Next, when combustion occurs, the combustion force $(F_p)_c$ becomes the most dominant. In combustion mode, a richer fuel-air mixture is introduced to obtain sustainable operation, while the integrated linear motor must work against some combustion pressure. The motoring forces should be gradually decreased until sustainable reciprocation is achieved. Finally, at the beginning of the power generation, when sustainable combustion events were achieved, the linear motor now acts as the generator.

Table 1. Summary of the three transient modes for a free-piston engine generator and the corresponding general equation of motion.

 Motoring mode	$$\sum F = F_{mot} + (F_p)_m - F_f - F_{cog}$$ $(F_p)_m$ is the resulting compression-expansion force.
 Starting mode	$$\sum F = F_{mot} + (F_p)_c - F_f - F_{cog}$$ $(F_p)_c$ is the resulting combustion force.
 Generating mode	$$\sum F = (F_p)_c - F_f - F_{cog}$$

These modes are important during the transient phase of the free-piston engine generator operation, with the forces were modelled differently by most researchers. Goldsborough and Blarigan [51] consider magnetic force resisting the motion during combustion, which is proportional to the translator speed. During generating, Mao [57] included electromagnetic force, which depends on motor constants.

3.2   A predictive stroke control approach

The absence of a crank-slider mechanism affects the stability of the cycle-to-cycle performance of free-piston engines. Each successive combustion event, especially in a dual-piston type FPE, relies on its previous stroke. This is further complicated by the adoption of a two-stroke cycle combustion mode, as each cylinder must contribute to another cylinder.

Factors such as scavenging performance, piston speed, compression ratio and combustion factors such as ignition and valve timings exemplify the complex endeavour facing FPEG researchers.

Predictive stroke control is a method of forecasting how the next stroke would be based on parameters such as the current stroke in-cylinder pressure with respect to the cyclic position. This is critical for a sustainable operation of the dual-piston type FPEG since one cylinder performance affect the other cylinder combustion and dynamics response.

Conventional crankshaft engines rely on crank angle degree (CAD) to map each stroke cylinder pressure profile. This is provided by a crank angle encoder sensor with gear teeth on the flywheel as it rotates. The crank angle degree referencing will complete 360° in every cycle consistently and this can be reset with a missing tooth on the flywheel. On the other hand, the free-piston engine has no rotational motion, and each stroke is not mechanically fixed. Therefore, an origin is set with each piston having the same distance from its respective cylinder head, as shown in **Fig. 3**. The piston position by cylinder 1 is defined for positive displacement, while cylinder 2 is for negative displacement.
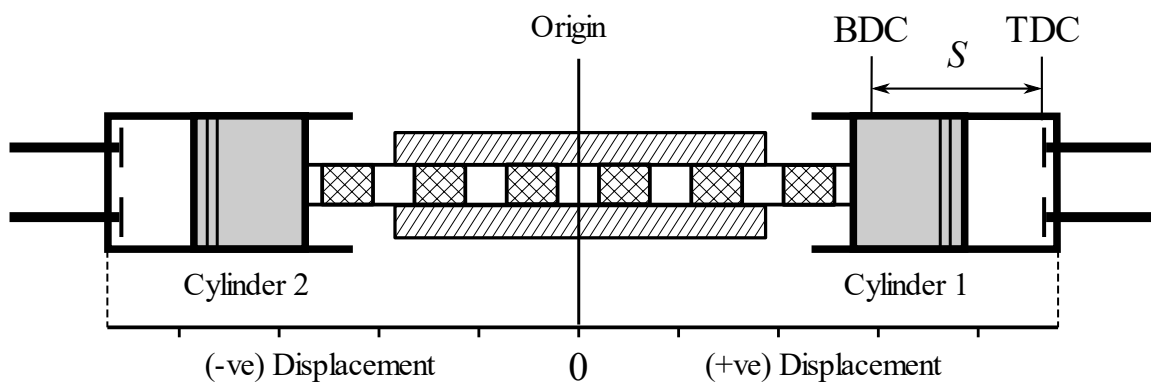
Fig. 3. Free-piston engine referencing for predictive stroke control.

In this way, a unique free-piston engine referencing is obtained from linear position readings, namely the cyclic position. The cyclic position provides time-independent representations of each FPE cycle, and this is similar to crank angle degree in crankshaft engine, which is useful in cyclic performance assessment. The illustrative details on this method are beyond the scope of this paper but can be obtained here [58]. Generally, cyclic position defines piston position referencing where the compression stroke from BDC to TDC is given as negative displacement values, starting from maximum stroke magnitude until zero, while expansion stroke from TDC to BDC is given as positive displacement values from zero to maximum stroke magnitude.

The cyclic position is calculated in real-time using the following formula:

$$x_{cyclic} = (x - x_{min}) * SIGN(v) \hspace{3cm} 37$$

Where x_{cyclic} is the cyclic position in mm, x is the real-time position of the piston during the stroke and x_{min} is the minimum piston position with respect to the TDC position of the previous stroke.

$SIGN(v)$ is the vector sign of the piston velocity; In this way, the induction/compression stroke will be negative, while the expansion/combustion stroke will be positive.

3.3 System configurations and specifications

The numerical model is based on a dual-piston type free-piston engine generator configuration, as shown in **Fig. 4**. A linear generator is integrated between two cylinders, with each cylinder having poppet valves for the gas exchange process. Both pistons are attached to a

translator shaft which contains north and south poles of permanent magnet pairs along its length. This translator passes through a set of stator coils as the main structure of the linear generator. Each cylinder combusts alternately in a two-stroke cycle operation providing necessary reciprocation to produce electrical power from the generator.
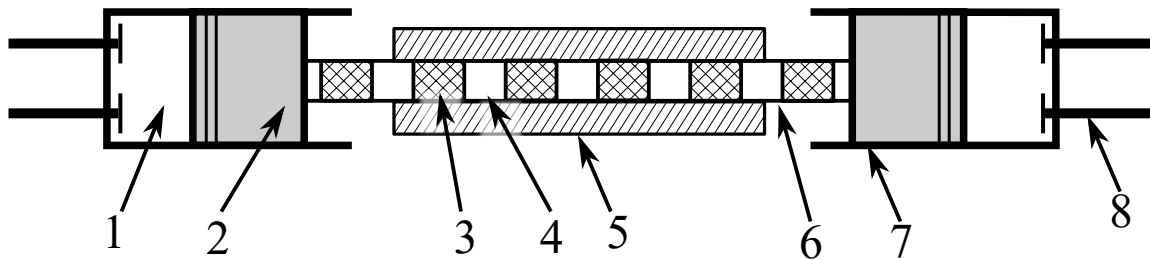

Fig. 4. The dual-piston type free-piston engine generator components- 1: Combustion chamber, 2: Piston, 3: North Pole permanent magnet, 4: South pole permanent magnet, 5: Stator coils, 6: Translator shaft, 7: Cylinder block, 8: Poppet valve for intake/exhaust.

Table 2. summarised the specifications for free-piston engine generator configurations. The bore of the cylinder is constant, while there are various stroke possibilities depending on operating variables. Nominal stroke is the median limit for producing a 10.5:1 compression ratio, which is typical for a spark-ignition engine. Each cylinder has different sized poppet valves for the intake and exhaust, while the valve timings were mapped based on piston position with respect to TDC.

Table 2. Engine specifications for the model.

	Free-piston Engine (FPE)
Bore [mm]	50.0
Stroke [mm]	38.0 (Nominal)
CR [1]	10.5:1 (Nominal)
Valve lift [mm]	4
Inlet valve diameter [mm]	16.5
Exhaust valve diameter [mm]	18.5
Intake valve open/close [mm bTDC]	24/33
Exhaust valve open/close [mm bTDC]	15/32
Clearance height [mm]	4.0

3.4 Model setup

The model utilises several sets of interactive zero-dimensional (zero-D) and one-dimensional (1-D)sub-models. Table 3 shows the essential sub-models for the integrated model. It allows the analysis of the dynamics of pressure waves, mass flows, and energy losses in ducts, plenums, and manifolds of the engine and provides a time-dependent solution of fluid dynamics and thermodynamics 1-D equations. By adding sub-models to simulate friction, heat transfer, scavenging, combustion, knock and exhaust emissions, this model is able to provide virtual investigations into FPEG transient operations. The piston motion sub-model provides a custom trajectory based on the intended motion profile for a typical free-piston. Additionally, a real-time calculated piston trajectory can be provided based on the motion dynamics.

Table 3. Zero-dimensional and one-dimensional sub-models.

Sub-model	Free-piston Engine (FPE)
Primary Combustion	SI-Wiebe
Zones	Two
Heat Transfer	Woschni Original
Friction	Chen-Flynn Friction
Knock	Douaud and Eyzat Model
Scavenging	Fully mix
Piston Motion	Custom/Calculated

Fig. 5 shows the model schematic for the interaction. Step 1 involves the initial speed and simulation duration setup. Step 2, the initial speed triggers either motoring, starting or generating sub-routines according to the transient modes. Each of the sub-routines contains relevant sub-models necessary for simulating the dynamics and combustions. Step 3 involves the motion dynamics, which calculate the piston position and velocity as well as cyclic position conversion in real-time. Finally, at stage 4, the results are saved for post-processing and data analyses. The adjustment of sub-routines is necessary for various engine speed simulations, compression ratio and knock activation.

①
Input initial cyclic speed (Hz)
Set simulation duration (s)

②
Mode selector: Motoring-Starting-Generating (autonomous)
Set TDC & Compression ratio targets
Sub-model activations:
>Gas Exchange
>Heat transfer (losses)
>Heat release (combustion)
>Two-zone combustion tracking (with knock prediction)

④
Post-processing data
Revise next TDC & compression ratio targets
Set threshold speed (Hz)
Repeat the simulation

③
Motion dynamics
Piston position tracking (real-time)
Cyclic position conversion (real-time)
Piston velocity tracking (real-time)
Actual vs. demand piston position comparison

Fig. 5. Schematic of real-time interaction model implementation Model schematic.

One-dimensional (1D) modelling of the internal combustion engines is an improved engine thermodynamics analysis that has been used for engine development by major automotive companies to assist prototype development due to its capability to produce realistic results quickly without the need for a three-dimensional computer-aided design (CAD) design of the engine.

WAVE is a 1D gas dynamics simulation tool software package developed by Ricardo which allows the performance analysis of internal combustion engines. **Fig. 6** shows the interaction structure between the 1D WAVE model subroutine and zero-dimensional MATLAB-Simulink model. WAVE model block is responsible for calculating the time-dependent solutions of fluid dynamics and thermodynamics 1D equations. The block transmits real-time in-cylinder pressure values of each FPEG cylinder for the zero-dimensional model dynamics motion calculations while the piston position is transmitted back into an imposed piston motion sub-model in WAVE.
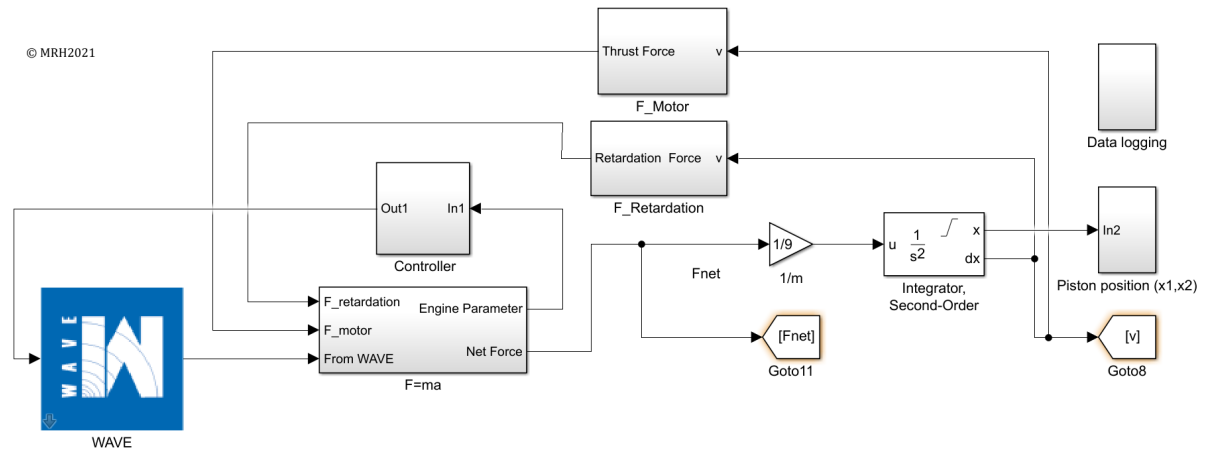
14

Fig. 6. The interactive sub-models of the dual-piston free-piston engine generator between 1-D WAVE sub-model and zero-D MATLAB-Simulink model.

The zero-dimensional model was established using MATLAB/Simulink as shown in **Fig. 7** to solve the numerical equations on piston dynamics, and linear motor/generator intervention for the predictive stroke control was possible using Stateflow. At the end of each simulation duration, various performance results were transferred to the workspace for post-processing and analyses. The investigation includes the impact of cyclic speed on FPEG performance, various compression ratios and knock responses.
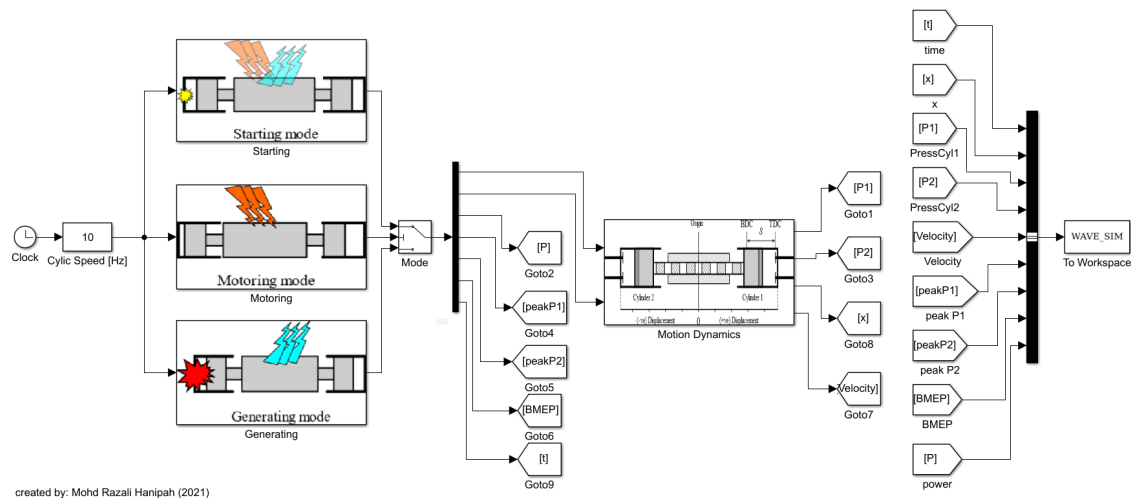
Fig. 7. Free-piston engine generator model developed in MATLAB-Simulink.

3.5 Model validations setup

The model validation is based on experimental data is obtained previously [19] from the FPEG prototype, as illustrated in **Fig. 8**. The prototype operates on a two-stroke spark ignition cycle as the combustion control is finite with spark ignition and the two-stroke cycle allows each cylinder to produce power alternately in succession for reciprocation. The piston position data was obtained from the linear position sensor, while the cylinder pressure data of both cylinders were provided by the spark plug pressure sensor.
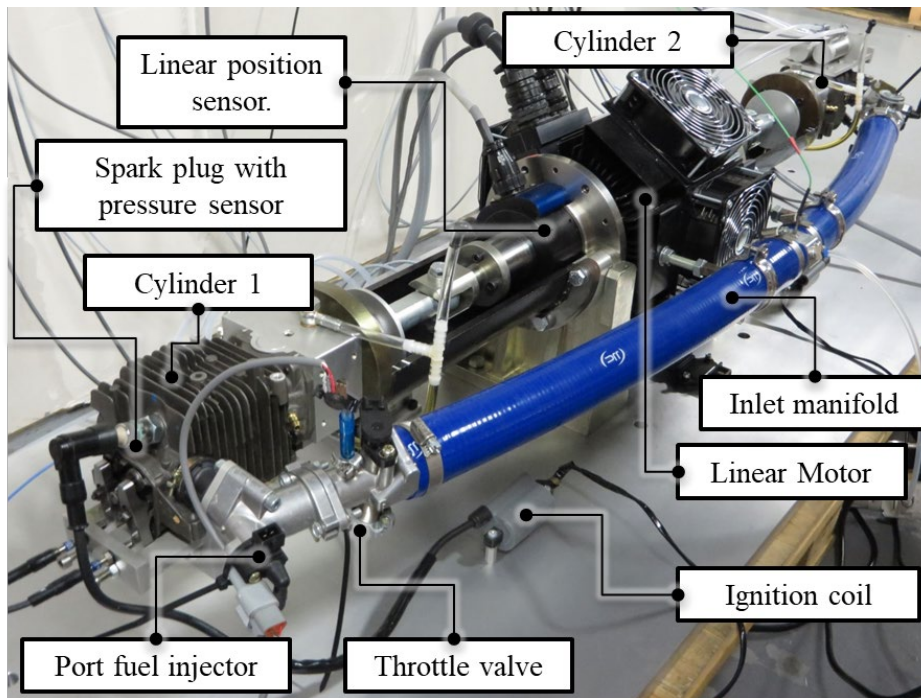
Fig. 8. Experimental setup used in acquiring the data for model validations [19].

The detailed layout for the prototype motion control and data acquisition systems is shown in **Fig. 9**. The system comprises of motor-driver operated through a workstation and a data acquisition system with an onboard controller operated through a host laptop during the experimentations.
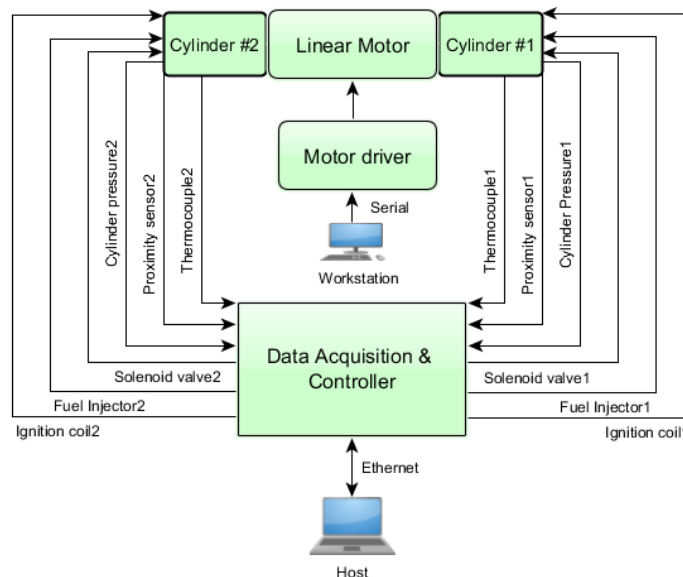

Fig. 9. The prototype data acquisition and controller schematic diagram [19].

4   Results and discussions

4.1   Model validation results

Fig. 10 (a) and (d) illustrates the correlation between the simulation and experimental results of the piston position and velocity profiles, respectively. The cycle starts from 41mm bTDC until 6mm bTDC for compression stroke and the return to BDC for the expansion stroke. A slight discrepancy was observed in piston position profiles during initial compression and

initial expansion stroke. This is manifested in a substantial piston velocity deviation in **Fig. 10** (a).

The possible reason for this deviation is because of the difference in motoring force application experienced by the actual prototype as the motion controller was trying to meet the targeted cyclic speed and stroke. Thus, for a realistic piston position profile, the motion control should be integrated into the simulation model as in hardware-in-the-loop (HIL), but this is beyond the scope of this paper.

Fig. 10 (b) shows the cylinder pressure profiles from the simulation during low-speed motoring, which reveals a good agreement with the experimental results. Cylinder leakage has been closely matched with different compression-expansion paths depicting the pumping losses during motoring. The peak cylinder pressure during 3Hz motoring shown is about 11bar. Similarly, the gas exchange period showing sudden pressure drop at the end of expansion stroke has been represented in the model.

The model included the actual intake and exhaust valve timing by matching the actual valve timing event from the experimental results. By plotting the pressure against the cyclic position as shown in **Fig. 10** (c), the compression and expansion pressure profile, as well as pressure fluctuation during exhaust blowdown (during scavenging period), could be assessed.

Overall, the difference between simulation and experiment results range between 2-5%. This is acceptable and allows for further exploration of the real-time model to observe the transient performance.
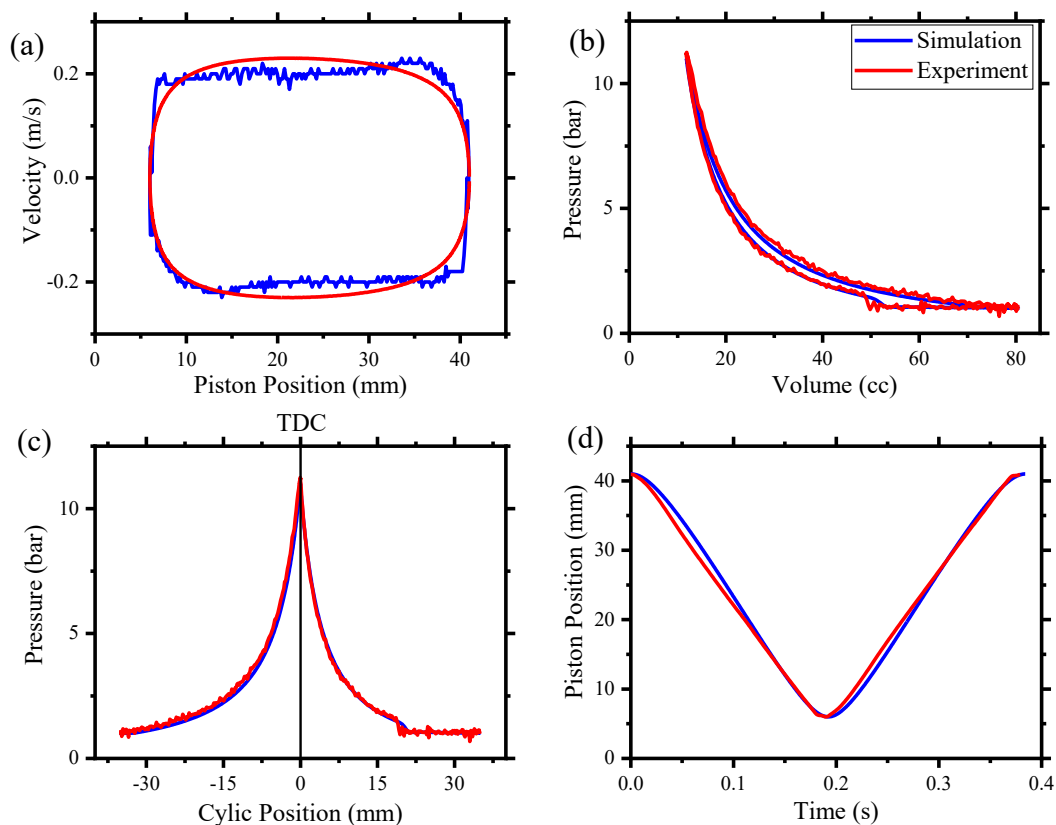

Fig. 10. Model validation results.

4.2 Performance prediction

Free-piston engines do not produce useful torque; hence the key performance parameters are brake thermal efficiency (bte), brake power (bpow) and brake mean effective pressure (bmep). The real-time model performance prediction is shown in **Fig. 11**. There are four cyclic speeds representing key transient phases of FPEG during operation. The starting speed of FPE is at 10Hz, which is equivalent to 600 rpm in a crankshaft engine. The model produced the lowest

17

power and efficiency at this speed which is consistent with a typical crankshaft engine since the gas exchange performance is very poor at low engine speed[4]. The bte and bpow show an increasing trend with increasing cyclic speed since power and efficiency are speed-dependent.
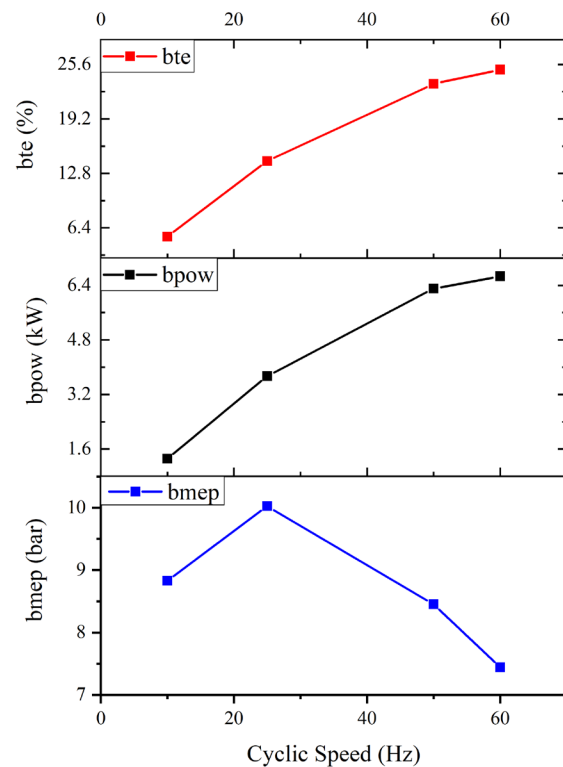

Fig. 11. Performance prediction at several cyclic speeds with a constant compression ratio.

The FPEG is aimed at the application of portable generators and series hybrid vehicles. Thus, its operational speed is finite and based on the electrical load demand and can be set to operate within a small range of cyclic speed. In this investigation, the target is to produce around 5kW at 50Hz, and the total engine capacity is about 150cc (around 75cc per cylinder) which will produce around 33 kW per litre in terms of power density while current IC engines can reach up to 50 kW per litre [59]. The targeted brake thermal efficiency (BTE) is around 20~30% at 50~60 Hz engine speed which has been shown achievable.

Fig. 12 shows the *pV* diagram for the same transient speed sweep. Lower transient speeds of 10 and 25 Hz produced higher combustion pressure around TDC but succumbed to considerable pumping loss at the end of the expansion stroke. The lower peak pressures at 50 and 60 Hz have contributed to the lower bmep values at these speeds, as observed in **Fig. 11**.
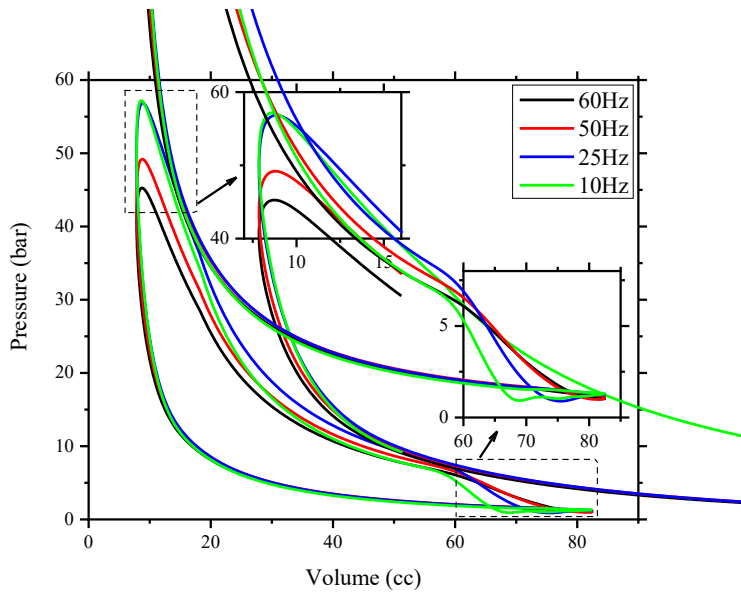
Fig. 12. *pV* diagram of the selected FPE transient speeds.

4.3 The impact of engine performance on piston motion

Fig. 13 shows the excess combustion energy which resulted in piston overshoot beyond the TDC target. In this cycle, the target stroke is 38mm with a 4mm clearance distance to achieve a compression ratio of 10.5:1. The cyclic speed is 50Hz which should follow the targeted motion profile. However, as the combustion produces excess energy, the resultant piston motion deviates and is overshot. This overshoot can cause catastrophic damage to the engine thus needs to be mitigated.
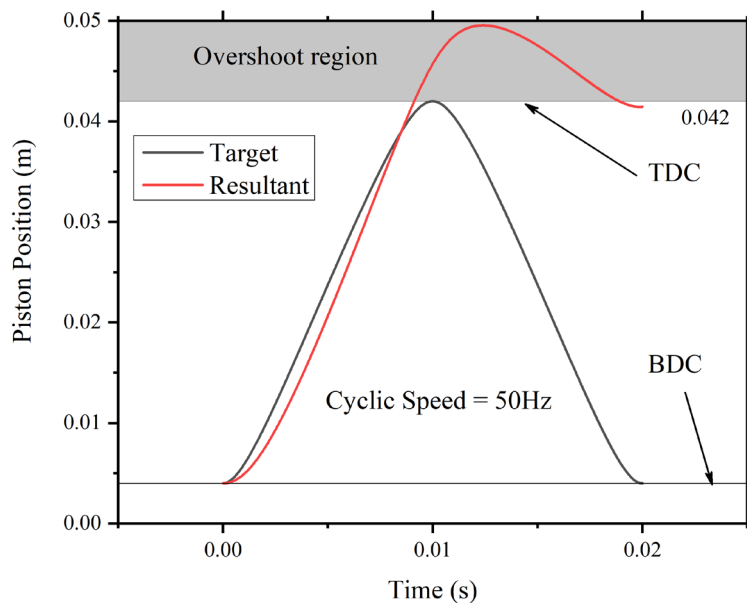
Fig. 13. Excess combustion energy piston overshoot.

On the other hand, **Fig. 14** shows the insufficient energy scenario when the model operates at 60Hz with less combustion energy, thereby reducing the resultant force. The piston motion followed a slower and deviated motion profile which caused the engine to stall. Both conditions are extreme cases and unwanted during the transient operation.

19

Predictive stroke control is proposed in this paper to mitigate these cases. The imposed piston motion control was deployed at 30% beginning of the stroke based on the information from cylinder pressure data. During this intervention, the integrated linear motor takes over to drive the piston towards TDC. Although the imposed motion profile deviates slightly, the piston has been successfully driven within 5% of the TDC position for the next cycle combustion event.
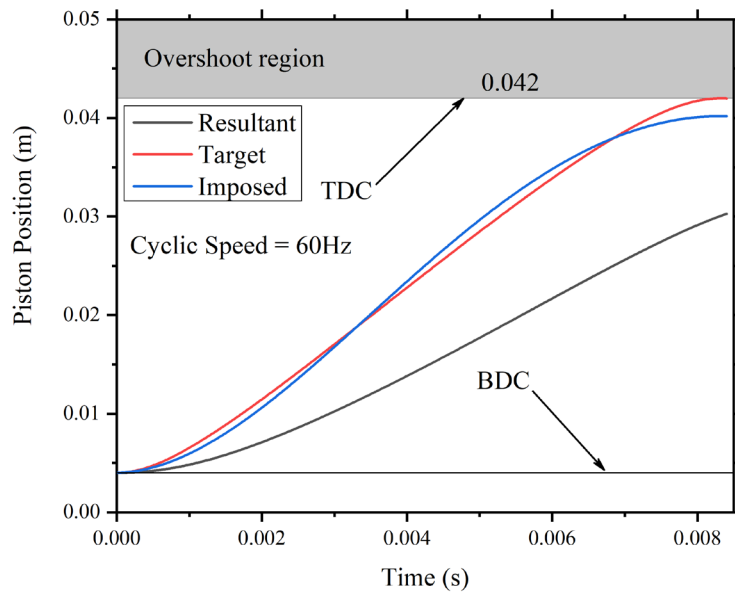

Fig. 14. Insufficient energy from combustion with predictive stroke motion control imposed.

Fig. 15 illustrates the three velocity profiles at 60Hz. The intended velocity profile is the target, while the result is the velocity produced by the piston motion dynamics based on the engine performance at 60Hz. The imposed velocity profile is a result of motoring force intervention which increase the net force and produce the acceleration required for the mitigation.
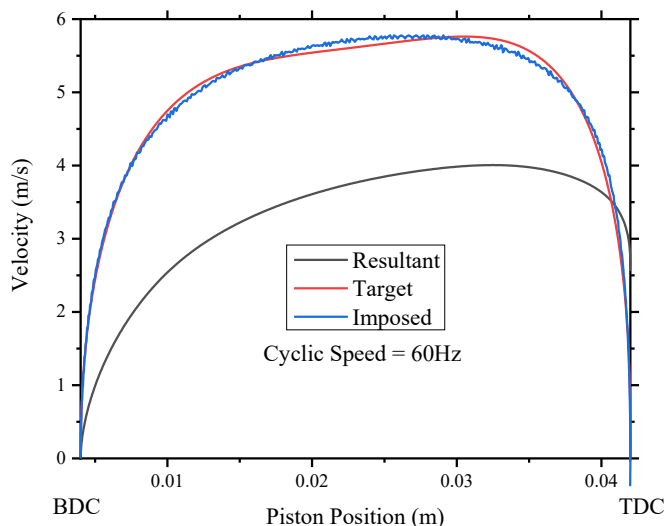
Fig. 15. Piston velocity profiles in mitigation scheme during insufficient combustion energy.

For the free-piston engine real-time monitoring system, the cyclic position has been proposed as the horizontal axis. **Fig. 16** depicts such a cyclic monitoring plot with in-cylinder pressure of various speeds plotted against the cyclic position. Since the cyclic position is a time-

independent variable, the pressure profiles at various engine speeds can be plotted and compared easily for evaluation. The negative cyclic position shows the compression stroke, while the positive side shows the combustion stroke. The result shows the highest pressure attained at 10Hz and 25Hz cyclic speeds, whereas lower cylinder pressure profiles are observed at 50 and 60Hz. These observations are consistent with the performance results presented in **Fig. 11**. Through this plot, the real-time assessment of cyclic performance is possible, and further intervention through ignition timing, fuel injection timing as well valve timings can be introduced in the motion control scheme in the future.
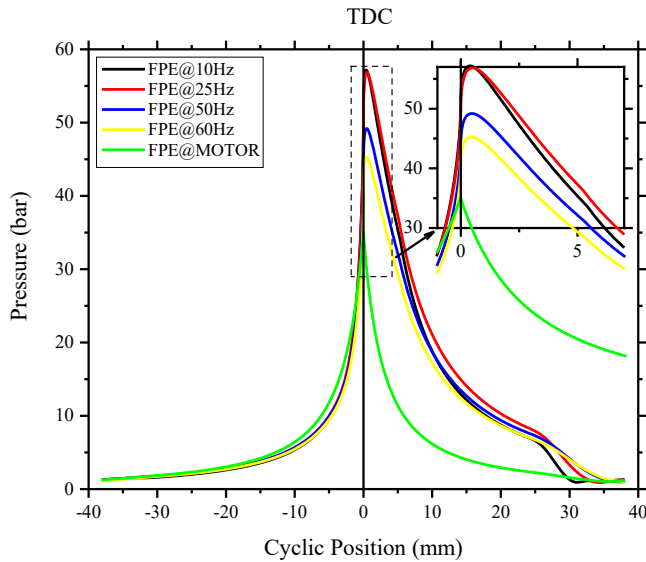
Fig. 16. Combustion pressure profiles at various cyclic frequencies were plotted against the cyclic position.

4.4   The impact of compression ratio and cyclic frequency on performance

In terms of engine performance, **Fig. 17** shows the brake thermal efficiency (bte) contours. Maximum bte of 25.8% lies in the mid-range of compression ratios between 10:1 to 15:1 while at the cyclic speeds of 50Hz to 60Hz. This result is consistent with the typical SI engine performance with regards to optimum compression ratio [4].
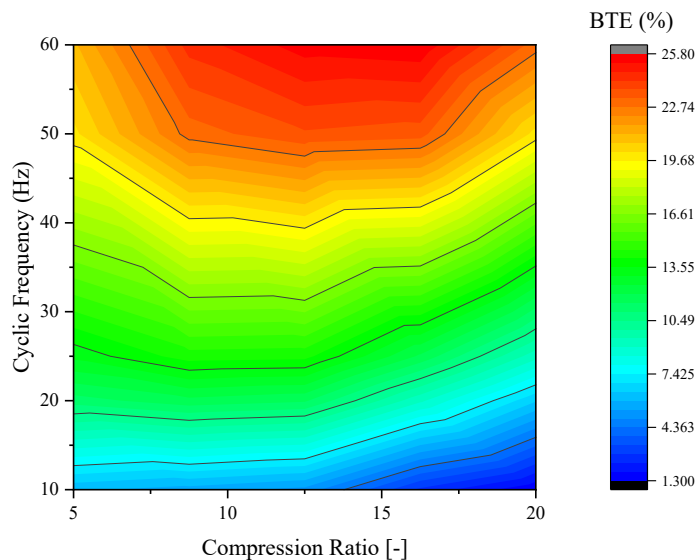
Fig. 17. Brake thermal efficiency response for various cyclic frequencies and compression ratios.

Fig. 18 shows a similar response is observed in brake power contour. Furthermore, the maximum brake power region at 50Hz is the best for compression ratios between 12:1 to 15:1.
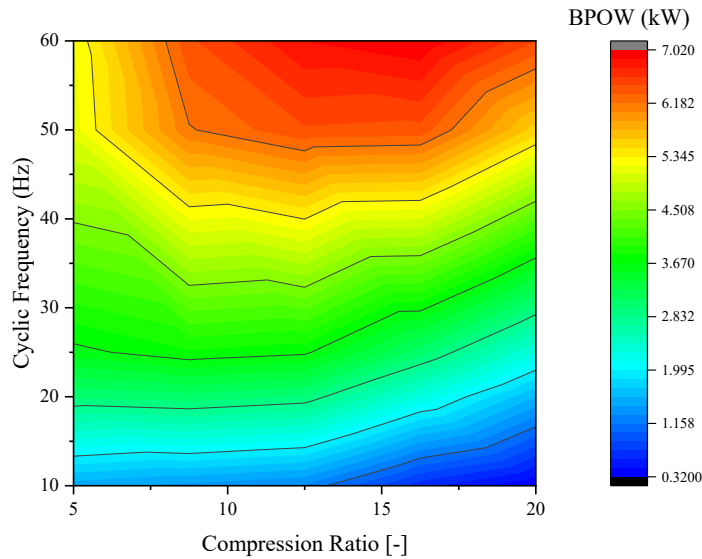

Fig. 18. Brake power response for various cyclic frequencies and compression ratios.

Fig. 19 shows the brake mean effective pressure contour where maximum bmep occurs between 5 to 12.5 compression ratios and corresponding speeds of 10 to 30 Hz. This result is consistent with typical brake torque response in similar sized crankshaft engines.
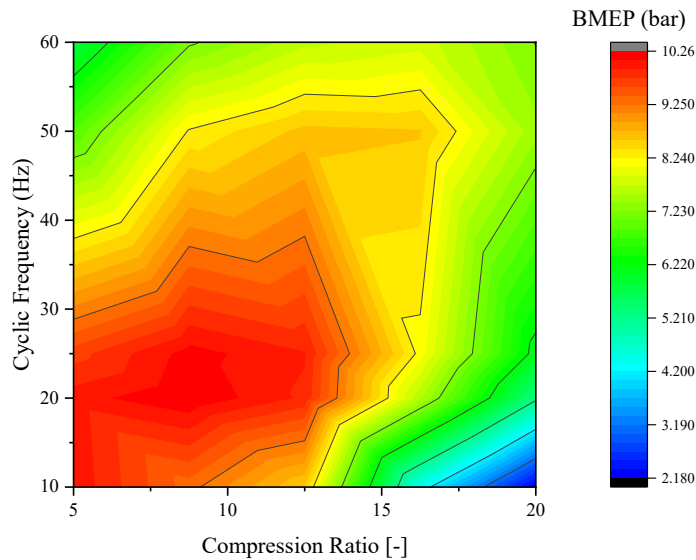

Fig. 19. Brake mean effective pressure response for various cyclic frequencies and compression ratios.

4.5 Knock predictions

Further investigations on the high cylinder pressure region exposed the knock events which occur at a high compression ratio. **Fig. 20** shows the pressure against time plot for the knock

incidence at 20:1 compression ratio and 50Hz cyclic speed. A similar pressure profile for normal combustion without knock is used as the baseline. The knock incidence resulted in poor engine performance, as observed previously.
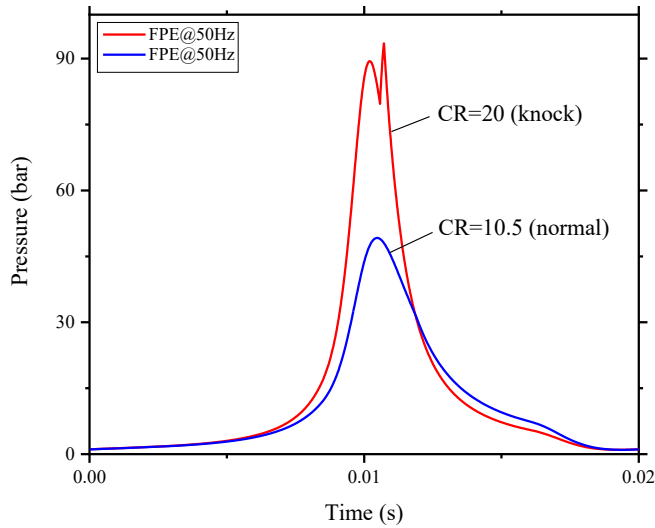

Fig. 20. In-cylinder pressure for normal and with knock event at 50Hz when the model was simulated at higher compression ratio.

Fig. 21 compares the time-independent plots for real-time engine performance monitoring. A typical crankshaft engine pressure profile is plotted against engine crank angle (CAD) as shown, while the proposed monitoring plot of pressure against the cyclic position is proposed for a free-piston engine. Zero CAD and zero mm represent TDC positions. Negative CAD and negative cyclic position represent compression stroke, while positive displacement and CAD represent the compression stroke.
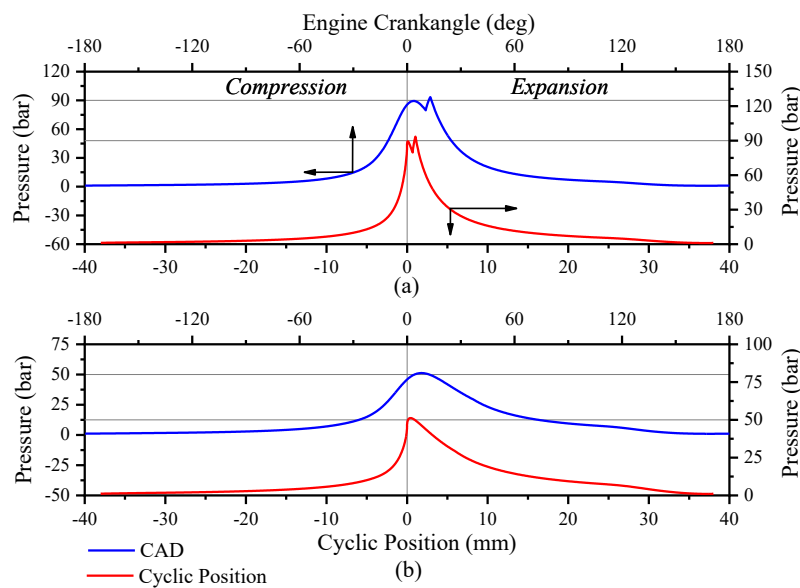

Fig. 21. The use of cyclic position for representing the cycle-to-cycle in-cylinder pressure profiles for real-time monitoring.

Fig. 22 shows pressure profiles for several knock events plotted against the cyclic position at various cyclic speeds. These are taken at CR of 20:1. As expected, the highest knock pressure occurs at 10Hz, while at 60Hz, the piston motion is fast enough to diminish the peak pressure generated due to knock.
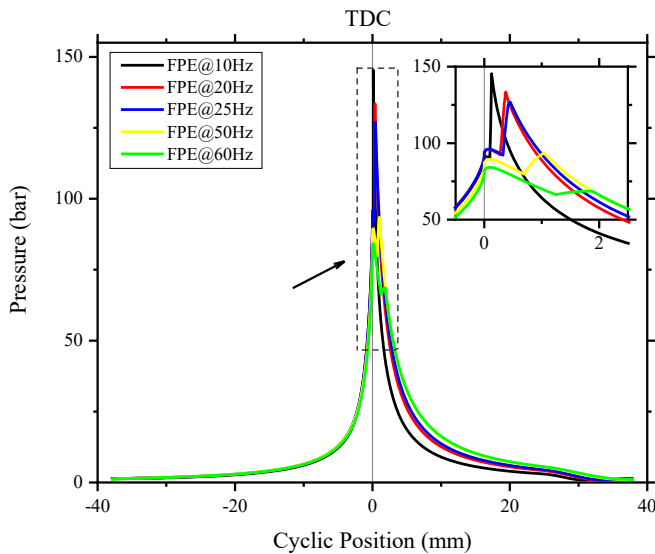

Fig. 22. In-cylinder pressure profiles during knock event at various cyclic speeds.

Fig. 23 shows the contour plot for the knock intensity distributions for various cyclic speeds and compression ratios. The result shows maximum knock intensity occurs at low cyclic speed when operated at a high compression ratio. It is proposed that the compression ratio should be below 12.0:1for knock-free operation during transience.
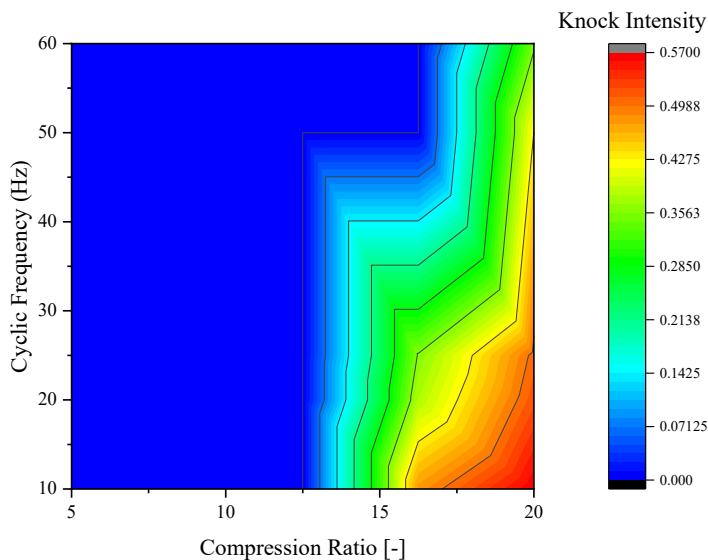

Fig. 23. The impact of cyclic frequency and compression ratio on the incident of knock event.

Fig. 24 shows the maximum cylinder pressure contour in response to the cyclic frequency and compression ratio, while the peak pressure contour shows a comparable response to the knock intensity contour. The maximum cylinder pressure occurs at the compression ratio of 20:1 and at the cyclic speed of 10Hz. This is expected as a high compression ratio will increase

the maximum cylinder pressure while slower cyclic speed allows for the cylinder pressure to rise.
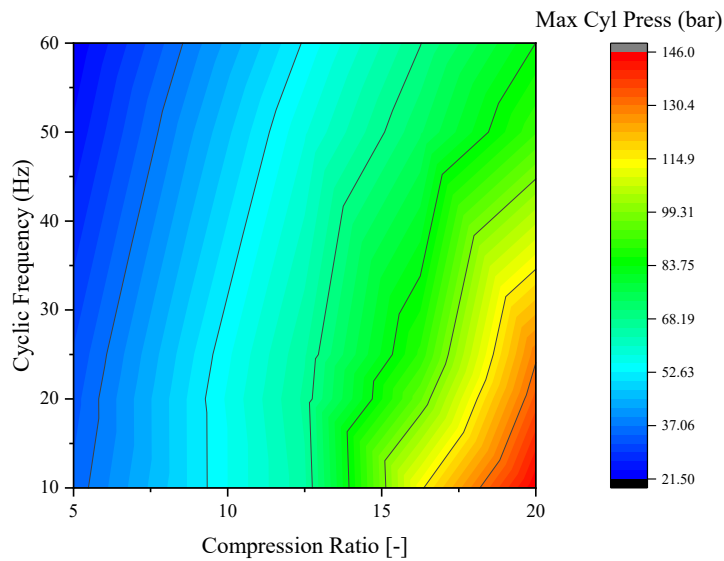

Fig. 24. Maximum cylinder pressure response for various cyclic frequencies and compression ratios.

5 Conclusions

This paper has presented a real-time interaction model of a dual-piston free-piston engine for transient operation performance investigations. The model involves interaction between dynamics of the piston motion and thermodynamics of the in-cylinder combustion. In this way, the negative impact of piston dynamics on combustion can be mitigated for sustainable operation.

A series of experimental results during motoring was used for validating the simulation model, which showed good agreement between simulation and experiment results with 2-5% errors. The targeted brake thermal efficiency is around 20~30% at 50~60 Hz engine speed which has been shown achievable. Transient speeds of 10 and 25 Hz produced higher combustion pressure around the top dead centre but suffered pumping loss at the end of the expansion stroke. The lower peak pressures at 50 and 60 Hz have contributed to the lower bmep brake mean effective pressure values. Maximum brake thermal efficiency of 25.8% lies in the mid-range of compression ratios between 10:1 to 15:1 while at the cyclic speeds of 50Hz to 60Hz. Maximum brake mean effective pressure contour occurs between 5 to 12.5 compression ratios and corresponding speeds of 10 to 30 Hz. Motoring, starting and generating are the three critical modes for the transient performance investigation. During each mode, two extreme conditions were observed. Excess energy from the combustion causes the piston to overshoot beyond the TDC, while insufficient energy prevents the piston from achieving the TDC and hence, the targeted compression ratio.

The model has successfully demonstrated performance response with respect to cyclic speed and compression ratio variations. Knock events were observed for low speed and high compression ratio cases. Knock occurs when the model operated at a higher compression ratio regardless of engine speed, affects the transient engine performance and must be resolved during actual operation. Predictive stroke control and knock detection capability are the main contribution of the real-time interaction model presented in this paper for realistic transient operation investigation and performance prediction of the dual-piston free-piston engine generator.

Acknowledgement

References

[1]   M. Razali Hanipah, R. Mikalsen, and A. P. Roskilly, "Recent commercial free-piston engine developments for automotive applications," *Appl. Therm. Eng.*, vol. 75, pp. 493–503, 2015.

[2]   C. Guo, Z. Zuo, H. Feng, B. Jia, and T. Roskilly, "Review of recent advances of free-piston internal combustion engine linear generator," *Appl. Energy*, vol. 269, no. January, p. 115084, Jul. 2020.

[3]   R. Stone, *Introduction to Internal Combustion Engines*, Third Edit. Warrendale, Pa.: Society of Automotive Engineers, Inc., 1999.

[4]   John Heywood, *John Heywood - Internal Combustion Engine Fundamentals-McGraw-Hill Education*. McGraw-Hill Education, 2018.

[5]   R. P. Pescara, "Motor Compressor Apparatus," 1928.

[6]   H. O. Farmer, "Free-Piston Compressor-Engines," *Proc. Inst. Mech. Eng.*, vol. 156, no. 1, pp. 253–271, 1947.

[7]   A. L. London and A. K. Oppenheim, "The free-piston engine development – Present status and design aspects," *Trans. ASME*, vol. 74, pp. 1349–1361, 1952.

[8]   P. A. J. Achten, "A review of free piston engine concepts," *SAE Tech. Pap.*, p. 941776, 1994.

[9]   P. A. J. Achten, J. P. J. van den Oever, J. Potma, and G. E. M. Vael, "Horsepower with Brains: The Design of the Chiron Free Piston Engine," *New Fluid Power Appl. Components, SAE Tech.*, vol. 2000-01–25, 2000.

[10]   R. Mikalsen and A. P. Roskilly, "A review of free-piston engine history and applications," *Appl. Therm. Eng.*, vol. 27, no. 14–15, pp. 2339–2352, 2007.

[11]   J. Hansson and M. Leksell., "Performance of a Series Hybrid Electric Vehicle with a Free-Piston Energy Converter," 2006.

[12]   T. J. Callahan1 and S. K. Ingram2, "Free-piston Engine Linear Generator for Hybrid vehicles modeling study," 1Southwest Research Institute, San Antonio, Texas & 2UT/Center for Electromechanics, The University of Texas, Austin, Texas, 1995.

[13]   H. Feng *et al.*, "Research on combustion process of a free piston diesel linear generator," *Appl. Energy*, vol. 161, pp. 395–403, 2016.

[14]   H. T. Aichlmayr, "Design Considerations, Modeling and Analysis of Micro-Homogeneous Charge Compression Ignition Combustion Free-Piston Engines.," UNIVERSITY OF MINNESOTA, 2002.

[15]   R. Huber, "Present state and future outlook of the free-piston engine," *Trans. ASME*, vol. 80, no. 8, pp. 1779–1790, 1958.

[16]   A. Hibi and T. Ito, "Fundamental test results of a hydraulic free piston internal combustion engine," *Proc. Inst. Mech. Eng. Part D J. Automob. Eng.*, vol. 218, no. 10, pp. 1149–1157, 2004.

[17]   P. Van Blarigan, N. Paradiso, and S. S. Goldsborough, "Homogeneous Charge Compression Ignition with a Free Piston: A New Approach to Ideal Otto Cycle Performance," *SAE Int.*, vol. 982484, 1998.

[18]   W. R. Cawthorne *et al.*, "Development of a linear alternator-engine for hybrid electric vehicle applications," *IEEE Trans. Veh. Technol.*, vol. 48, no. 6, pp. 1797–1802, 1999.

[19]   M. R. Hanipah, "Development of a spark ignition free-piston engine generator," no. June, 2015.

[20]   S. Tikkanen, M. Lammila, M. Herranen, and M. Vilenius, "First cycles of the dual hydraulic

free piston engine," *SAE Tech. Pap.*, no. 724, 2000.

[21]   P. Van Blarigan and J. O. Keller., "A Hydrogen Fuelled Internal Combustion Engine Designed fro Single Speed/Power Operation," *Int. J. Hydrogen Energy*, vol. 23., 1998.

[22]   S. S. Goldsborough and P. Van Blarigan, "A Numerical Study of a Free Piston IC Engine Operating on Homogeneous Charge Compression Ignition Combustion," *SAE Int.*, vol. 1999-01–06, 1999.

[23]   P. Brejaud, P. Higelin, A. Charlet, G. Colin, and Y. Chamaillard, "One Dimensional Modeling and Experimental Validation of Single Cylinder Pneumatic Combustion Hybrid Engine," *SAE Int. J. Engines*, vol. 4, no. 2, pp. 2326–2337, 2011.

[24]   J. Fredriksson and I. Denbratt, "Simulation of a Two-Stroke Free Piston Engine," *SAE Int.*, vol. 2004-01–18, 2004.

[25]   M. Erland, "FPEC, Free Piston Energy Converter," in *EVS21, Proceedings of the 21st Electric Vehicle Symposium & Exhibition*, 2005.

[26]   R. Mikalsen and A. P. Roskilly, "Performance simulation of a spark ignited free-piston engine generator," *Appl. Therm. Eng.*, vol. 28, no. 14–15, pp. 1726–1733, 2008.

[27]   R. Mikalsen and A. P. Roskilly, "The design and simulation of a two-stroke free-piston compression ignition engine for electrical power generation," *Appl. Therm. Eng.*, vol. 28, no. 5–6, pp. 589–600, 2008.

[28]   B. Jia, R. Mikalsen, A. Smallbone, Z. Zuo, H. Feng, and A. P. Roskilly, "Piston motion control of a free-piston engine generator: A new approach using cascade control," *Appl. Energy*, vol. 179, pp. 1166–1175, 2016.

[29]   R. Mikalsen, E. Jones, and A. P. Roskilly, "Predictive piston motion control in a free-piston internal combustion engine," *Appl. Energy*, vol. 87, no. 5, pp. 1722–1728, 2010.

[30]   R. Mikalsen and A. P. Roskilly, "The control of a free-piston engine generator. Part 1: Fundamental analyses," *Appl. Energy*, vol. 87, no. 4, pp. 1273–1280, 2010.

[31]   S. A. Zulkifli, M. N. Karsit, and A. R. A. Aziz, "Rectangular current commutation and open-loop control for starting of a free-piston linear engine-generator," *PECon 2008 - 2008 IEEE 2nd Int. Power Energy Conf.*, pp. 1086–1091, 2008.

[32]   S. A. Zulkifli, M. N. Karsiti, and A. R. A. Aziz, "Investigation of linear generator starting modes by mechanical resonance and rectangular current commutation," in *2009 IEEE International Electric Machines and Drives Conference*, 2009, pp. 425–433.

[33]   P. Němeček and OndřejVysoký, "Control of Two-Stroke Free-Piston Generator," *Proc. 6th Asian Control Conf.*, vol. VOL.1, 2006.

[34]   P. Deutsch and O. Vysoký, "The Free-Piston Engine model in Matlab/Simulink," *MECCA J. Middle Eur. Constr. Des. Cars*, vol. VOL.5, 2007.

[35]   B. Jia, Y. Wang, A. Smallbone, and A. Roskilly, "Analysis of the Scavenging Process of a Two-Stroke Free-Piston Engine Based on the Selection of Scavenging Ports or Valves," *Energies*, vol. 11, no. 2, p. 324, 2018.

[36]   R. Mikalsen and A. P. Roskilly, "The control of a free-piston engine generator. Part 2: Engine dynamics and piston motion control," *Appl. Energy*, vol. 87, no. 4, pp. 1281–1287, 2010.

[37]   S. Nandkumar, "Two-Stroke Linear Engine," West Virginia University, Morgantown, West Virginia, 1998.

[38]   M. Z. Saiful Azrin, "Modeling, Simulation and Implementation of Rectangular Commutation for Starting of Free-Piston Linear Generator," Universiti Teknologi PETRONAS, 2007.

[39]   T. A. Johansen, O. Egeland, E. A. Johannessen, and R. Kvamsdal, "Free-piston diesel engine dynamics and control," in *American Control Conference*, 2001, vol. 6, pp. 4579–4584 vol.6.

[40]   P. Němeček, M. Šindelka, and O. Vysoký, "Modeling and Control of Linear Combustion Engine," *IFAC Symp. Adv. Automot. Control.*, 2003.

[41]   Z. Xu and S. Chang, "Prototype testing and analysis of a novel internal combustion linear generator integrated power system," *Appl. Energy*, vol. 87, no. 4, pp. 1342–1348, 2010.

[42]   B. Jia, A. Smallbone, Z. Zuo, H. Feng, and A. P. Roskilly, "Design and simulation of a two- or four-stroke free-piston engine generator for range extender applications," *Energy*

Convers. Manag., vol. 111, pp. 289–298, 2016.

[43] S. Petreanu, "Conceptual Analysis of A Four-Stroke Linear Engine," West Virginia University, Morgantown, West Virginia, 2001.

[44] T. A. Johansen, O. Egeland, E. A. Johannessen, and R. Kvamsdal., "Free-Piston Diesel Engine Dynamics and Control," *Proc. Am. Control Conf.*, 2001.

[45] C. M. Atkinson, R. J. Atkinson, T. I. McDaniel, S. Nandkumar, and P. Famouri, "Numerical Simulation of a Two-Stroke Linear Engine-Alternator Combination," *SAE Int. Hybrid Veh. Engines Fuel Technol.*, vol. 1999-01–09, 1999.

[46] S. S. Goldsborough and P. Van Blarigan, "A numerical study of a free piston IC engine operating on homogeneous charge compression ignition combustion," *SAE Tech. Pap.*, no. 724, 1999.

[47] J. Marsh, "Motor Parameters Application Note," 2003. [Online]. Available: http://www.parkermotion.com/whitepages/linear_motor_parameter_application_note.pdf.

[48] S. A. Zulkifli, M. N. Karsiti, and A. R. A. Aziz, "Starting of a free-piston linear engine-generator by mechanical resonance and rectangular current commutation," in *Vehicle Power and Propulsion Conference, 2008. VPPC '08. IEEE*, 2008, pp. 1–7.

[49] M. R. Hanipah, "Combustion process in a Two-Stroke, H2-DI Linear Generator Free-Piston Engine during starting.," Universiti Teknologi PETRONAS, Tronoh, Perak, Malaysia., 2008.

[50] G. P. Blair, *Design and Simulation of Two-Stroke Engines*. Warrendale, PA: SAE Inc., 1996.

[51] S. S. Goldsborough and P. Van Blarigan, "A Numerical Study of a Free Piston IC Engine Operating on Homogeneous Charge Compression Ignition Combustion." SAE International, 1999.

[52] S. K. and P. F. F. Chen, "Development of Single Cylinder Compression Ignition Research Engine," *SAE Tech. Pap. 650733*, 1965.

[53] G. P. Blair and G. P. Blair, *Two-Stroke Engines*. .

[54] W. W. Pulkrabek, *Engineering Fundamentals of the Internal Combustion Engine*. Prentice-Hall, Inc., 1997.

[55] A. M. Douaud and P. Eyzat, "Four-Octane-Number Method for Predicting the Anti-Knock Behavior of Fuels and Engines," *SAE Tech. Pap.*, Feb. 1978.

[56] R. D. Matthews, "Relationship of brake power to various energy efficiencies and other engine parameters: the efficiency rule," *Int. J. Veh. Des.*, vol. 4, no. 5, pp. 491–500, 1983.

[57] J. L. Mao, Z. X. Zuo, and H. H. Feng, "Parameters coupling designation of diesel free-piston linear alternator," *Appl. Energy*, vol. 88, no. 12, pp. 4577–4589, 2011.

[58] M. Razali Hanipah, M. Haziq Adham Rosli, and A. R. Razali, "A New Piston Referencing Algorithm for Qualitative Assessment of Free-Piston Engine Generator Performance," in *Lecture Notes in Mechanical Engineering*, 2021, vol. 46.

[59] Chris Mi, M. Abul Masrur, and D. W. Gao., *Hybrid Electric Vehicles: Principles and Applications with Practical Perspectives*. John Wiley & Sons, Ltd, 2011.